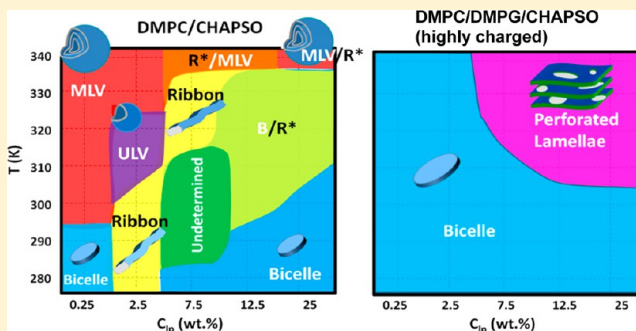


Morphological Characterization of DMPC/CHAPSO Bicellar Mixtures: A Combined SANS and NMR Study

Ming Li,[†] Hannah H. Morales,[‡] John Katsaras,^{§,||,⊥,♯} Norbert Kučerka,[▽] Yongkun Yang,[†] Peter M. Macdonald,^{*,‡} and Mu-Ping Nieh^{*,†,○}[†]Polymer Program, Institute of Materials Science, University of Connecticut, Storrs, Connecticut 06269, United States[‡]Department of Chemical and Physical Sciences, University of Toronto Mississauga, Mississauga, Ontario L5L 1C6, Canada[§]Biology & Soft Matter Division, Neutron Sciences Directorate and ^{||}Joint Institute for Neutron Sciences, Oak Ridge National Laboratory, Oak Ridge, Tennessee 37831, United States[⊥]Department of Physics and Astronomy, University of Tennessee, Knoxville, Tennessee 37996-1200, United States[♯]Department of Physics, Brock University, St. Catharines, Ontario L2S 3A1, Canada[▽]Canadian Neutron Beam Centre, National Research Council, Chalk River, Ontario K0J 1J0, Canada[○]Department of Chemical & Biomolecular Engineering and Department of Biomedical Engineering, University of Connecticut, Storrs, Connecticut 06269, United States

S Supporting Information

ABSTRACT: Spontaneously forming structures of a system composed of dimyristoyl phosphatidylcholine (DMPC) and 3-[(3-cholamidopropyl)dimethylammonio]-2-hydroxy-1-propanesulfonate (CHAPSO) were studied by small-angle neutron scattering (SANS), ³¹P NMR, and stimulated echo (STE) pulsed field gradient (PFG) ¹H NMR diffusion measurements. Charged lipid dimyristoyl phosphatidylglycerol (DMPG) was used to induce different surface charge densities. The structures adopted were investigated as a function of temperature and lipid concentration for samples with a constant molar ratio of long-chain to short-chain lipids (= 3). In the absence of DMPG, zwitterionic bicellar mixtures exhibited a phase transition from discoidal bicelles, or ribbons, to multilamellar vesicles either upon dilution or with increased temperature. CHAPSO-containing mixtures showed a higher thermal stability in morphology than DHPC-containing mixtures at the corresponding lipid concentrations. In the presence of DMPG, discoidal bicelles (or ribbons) were also found at low temperature and lower lipid concentration mixtures. At high temperature, perforated lamellae were observed in high-concentration mixtures (≥7.5 wt %) whereas uniform unilamellar vesicles and bicelles formed in low-concentration mixtures (≤2.5 wt %), respectively, when the mixtures were moderately and highly charged. From the results, spontaneous structural diagrams of the zwitterionic and charged systems were constructed.



■ INTRODUCTION

Bicellar mixtures consisting of detergents and phospholipids are capable of assuming a number of morphologies. At low temperature, the phospholipids assemble into disc-like single bilayer planar fragments (bicelles), which are edge-stabilized by the detergent molecules. Discoidal bicelles are intermediate in size and fall between small, highly curved detergent micelles and extended lamellar bilayers made up of phospholipids. It is thought that the bicelle's planar bilayer region is a better mimic of membrane proteins to interact or reside in, than, for example, the highly curved surface of a detergent micelle. Consequently, bicelles have become increasingly popular in structural studies of membrane proteins, particularly those studied by nuclear magnetic resonance (NMR), and have been the subject of numerous reviews regarding their properties and uses.^{1–11}

Beyond NMR studies, bicelles are being used in a broader range of applications, such as in electron paramagnetic resonance (EPR) studies of embedded membrane proteins,^{12–14} as media for improving the crystallization of membrane proteins for X-ray structure studies,^{15–17} as membrane protein¹⁸ and drug delivery vehicles,¹⁹ and as precursors in the formation of bilayer coatings on polymeric substrates.²⁰ However, much of their popularity has been derived as a result of their rich morphological repertoire, which is induced by the phospholipid/detergent ratio (*Q*), lipid concentration (*C_{lip}*), and temperature. For example, large amounts of detergent produce small, isotropically tumbling

Received: July 24, 2013

Revised: September 12, 2013

Published: September 23, 2013

planar discs, which are amenable to solution-state NMR studies of membrane-associated proteins or of soluble proteins interacting with the lipid bilayer.^{7–10} With increasing temperature and C_{lp} , the bilayered micelle morphology converts to wormlike, chiral nematic ribbons and eventually to extended lamellae populated with detergent-coated perforations. This latter morphology has the propensity to align in a magnetic field, a property that lends these systems to studies of membrane proteins by solid-state NMR^{1–3,5,7,11} and as an orientationally aligning medium for solution-state NMR studies of soluble proteins.^{7,11}

Much of what has been established concerning the morphological transformations experienced by bicelles has been through small-angle neutron scattering (SANS) studies,^{6,21,22} aided and abetted by NMR^{23–27} and electron microscopy.²⁸ Most of these studies were performed using the canonical bicellar mixture introduced by Sanders and Schwonek²³ (i.e., short-chain phospholipid dihexanoyl phosphatidylcholine (DHPC) with dimyristoyl phosphatidylcholine (DMPC)). Although early reports on bicelles used bile salt 3-(cholamidopropyl)dimethyl-ammonio-2-hydroxyl-1-propane-sulfonate (CHAPSO) instead of DHPC as the detergent component,^{29,30} over the years CHAPSO has been largely displaced by DHPC, resulting in a bicellar mixture consisting entirely of phospholipids. CHAPSO, however, is known to confer certain advantages, such as, imparting better functionality to bicelle reconstituted membrane proteins,^{31,32} and enhanced pH³³ and thermal stability in terms of morphology,^{33,34} compared to DHPC-containing mixtures. Nevertheless, comparisons of DHPC- versus CHAPSO-containing bicelles reveal that they also have much in common, such as the formation of bicelle discs at high concentrations and the ability of assemblies of molecules to orient in a magnetic field at higher lipid concentrations and temperatures above the gel to liquid-crystalline phase transition of DMPC.²⁹ However, to the best of our knowledge SANS studies of CHAPSO-containing bicelles have yet to be carried out, and the structural phase diagram of DMPC/CHAPSO mixtures has yet to be resolved. Thus, it is not clear whether, and to what extent, CHAPSO-containing bicelles undergo morphological transformations analogous to those observed in DHPC-containing bicelles.

In this report, SANS is used to investigate the morphologies of $Q = \text{DMPC}/\text{CHAPSO} = 3$ bicellar mixtures as a function of lipid concentration, temperature, and the presence of the negatively charged phospholipid, dimyristoyl phosphatidylglycerol (DMPG). A comparison is made to corresponding DHPC-containing bicelles. For 25 wt % lipid mixtures, where magnetic orientation is readily achieved,³¹ ^{31}P NMR was used to characterize the quality of magnetic alignment, and ^1H pulsed field gradient (PFG) NMR diffusion studies were conducted to understand the bicellar structural and dynamic behavior. The SANS and NMR techniques provide a consistent picture of the bicelle morphology as a function of temperature, lipid concentration, and surface charge density (molar ratio of DMPG). Although the general trend in morphological transformations of CHAPSO-containing bicelles mirrors those undergone by DHPC-containing bicelles, CHAPSO is shown to impart significantly greater thermal stability to morphologies with high-curvature defects.

MATERIALS AND METHODS

Sample Preparation. DMPC, DHPC, and DMPG were purchased from Avanti Polar Lipids (Alabaster, AL). CHAPSO used for SANS and

NMR studies was purchased from Sigma-Aldrich (St. Louis, MO) and Avanti Polar Lipids, respectively. All chemicals were used without further purification. Figure 1 shows the chemical structures of DHPC

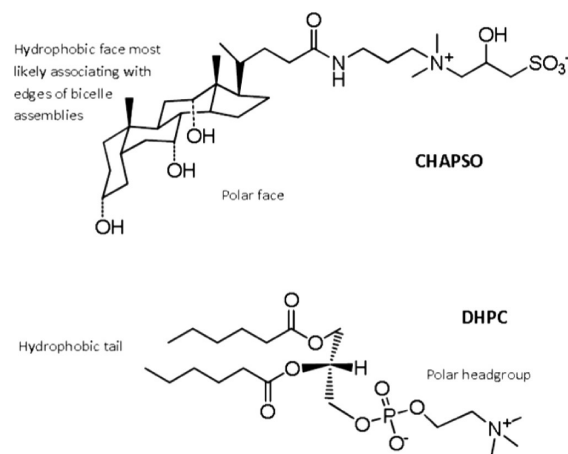


Figure 1. Chemical structures of CHAPSO and DHPC.

and CHAPSO. Although both molecules contain hydrophilic and hydrophobic regions, the difference in molecular architecture enables the formation of the different morphologies.

For SANS measurements, CHAPSO-containing mixtures with various molar ratios of charged to total long-chain lipid, $R = [\text{DMPG}]/([\text{DMPC}] + [\text{DMPG}])$, were prepared, specifically, $R = 0$, 0.01 and 0.10 but with a constant molar ratio of long-chain lipid to detergent ($Q = ([\text{DMPC}] + [\text{DMPG}])/[\text{CHAPSO}] = 3$). For each, the appropriate amounts of a given dry lipid powder were combined and hydrated in D_2O (99.8% purity, Cambridge Isotope Laboratories, Inc., Andover, MA) to make a stock solution of $C_{lp} = 25$ wt %. Dispersion was achieved by temperature cycling between low ($\sim 4^\circ\text{C}$) and high (40 – 50°C) temperatures, in combination with vortex mixing. Hydration was judged to be complete when stock solutions became completely transparent and liquidlike at low temperature ($T < 20^\circ\text{C}$). Upon heating, stock solutions became viscous and translucent, or in the absence of DMPG turned opaque. All of these phenomena were reversible with temperature and similar to the behavior reported in DMPC/DHPC mixtures.^{21–26} For each R value, the stock solution was further diluted to $C_{lp} = 12.5$, 7.5, 2.5, and 0.25 wt %. For comparative purposes, a bicellar mixture of DMPC/DHPC with $Q = 3$ and $C_{lp} = 25$ wt % was also prepared in the manner described.

For NMR experiments, an identical set of CHAPSO-containing mixtures was prepared with $R = 0$, 0.01, and 0.10 at $C_{lp} = 25$ wt %. Poly(ethylene glycol) with an average molecular weight of 1000 Da (PEG-1000) was incorporated into the bicelle mixtures as a diffusion probe. PEG-1000 was added from an aqueous stock solution to a final concentration of 0.8 mol % with respect to DMPC. The addition was performed subsequent to bicelle formation and at a temperature where the bicelle sample was least viscous (i.e., 4°C for DHPC-containing and 10 – 15°C for CHAPSO-containing bicelles). At this molecular weight and concentration, the added PEG exerted no discernible perturbation of the bicelle properties, including their ability to align in a magnetic field.

SANS Measurements and Analysis. SANS measurements were performed using the N5 spectrometer located at the National Research Universal (NRU) reactor (Chalk River Laboratories, Ontario, Canada) and the Bio-SANS (CG3) instrument at Oak Ridge National Laboratory (ORNL, Oak Ridge, TN, USA). The scattering intensity, I , was collected as a function of scattering vector, q , defined as $q = (4\pi)/\lambda \sin(\theta/2)$, where λ and θ are the neutron wavelength and scattering angle, respectively. To cover a q range of between 0.006 and 0.2 \AA^{-1} at N5, three different wavelengths were used, specifically, $\lambda = 1.55$, 2.37, and 3.99 \AA . The incident beam was focused with a multichannel focusing collimator, and a “de-smearing” collimator was installed to reduce the vertical divergence on the scattering side. A detailed description of the

optical configuration and instrumental resolution has been previously reported.³⁵ At CG3, the wavelength was fixed at 6 Å and the sample-to-detector distance was set to 6 m, covering a q range from 0.005 to 0.15 Å⁻¹. The temperature of the sample stage, at both facilities, was controlled by a circulating water bath. The temperature gradient between the sample and water bath readout was usually less than 2 °C.

Generally speaking, the SANS scattering intensity, $I(q)$, for a system containing one type of particle (morphology) is proportional to the product of the form factor (shape of the particle), $P(q)$, and the structure factor (the interaction between particles), $S(q)$. Mathematically, $P(q)$ is derived from the square of the Fourier transform of the scattering density fluctuations taking place in the system (i.e., the Fourier transform of the morphology, e.g., disc, vesicle, micelle, etc.). In the case of high-concentration samples, strong interparticle interactions are expected, and $S(q)$ can no longer be neglected. Several models of $P(q)$ including, disc, ribbons, and unilamellar vesicles (Supporting Information) were used to fit the scattering intensities for low-concentration samples, where $S(q)$'s contribution was negligible. The fitting program was developed at the National Institute of Standards and Technology (NIST) Center for Neutron Research (NCNR) in Gaithersburg, MD, USA.³⁶ In the case of concentrated samples, where strong Bragg diffraction peaks, as a result of positionally correlated bilayers, are present, a phenomenological model, as expressed in eq 1, was used to fit the SANS data in order to determine the interlamellar spacing, or d spacing.³⁷ The model assumes that Bragg peaks sit on top of the background signal, which, depending on the q range, contains two distinct slopes (i.e., $-m$ and $-n$) in the low- and high- q regimes, respectively, as described in the first term on the r.h.s. of eq 1

$$I(q) = \frac{s_0}{(1 + s_1 q^m + s_2 q^n)} + p_1 \exp\left[\frac{-(q - q_1)^2}{\sigma_1^2}\right] + p_2 \exp\left[\frac{-(q - q_2)^2}{\sigma_2^2}\right] + \text{BGD} \quad (1)$$

where s_0 , s_1 , and s_2 are constants, and the two Gaussian peaks are located at $q = q_1$ and q_2 , having peak widths of σ_1 and σ_2 , respectively. The BGD term represents the incoherent background scattering, and $2\pi/q_1 = d$.

NMR Spectroscopy. All NMR spectra were recorded on a Varian Infinity 500 MHz NMR spectrometer using a Varian 5 mm double-resonance liquid probe equipped with gradient coils along the z direction. The sample temperature was controlled to within ± 0.5 K of the desired value, as calibrated using ethylene glycol. Bicelle samples were transferred to an NMR tube at a temperature corresponding to the particular viscosity minimum of 4 °C for DHPC-containing mixtures, and 15 °C for CHAPSO-containing mixtures. To encourage magnetic alignment after being placed into the NMR spectrometer, the bicellar mixtures were annealed by repeatedly cycling the temperature between 25 and 35 °C. The quality of alignment was assessed via both ²H and ³¹P NMR spectroscopy.

²H NMR spectra were recorded at 76.72 MHz using single-pulse excitation with quadrature detection. Typical parameters used were a 90° pulse length of 10 μs, a recycle delay of 100 ms, a spectral width of 1250 Hz, and a 4K data size. Spectra were processed with an exponential multiplication equivalent to 5 Hz of line broadening prior to Fourier transformation.

³¹P NMR spectra were recorded at 202.31 MHz using single-pulse excitation, quadrature detection, CYCLOPS phase cycling, and WALTZ proton decoupling during signal acquisition with a proton decoupler field strength of 4 kHz. The data were acquired using the following typical parameters: a 90° pulse length of 16 μs, a recycle delay of 1 s, a spectral width of 100 kHz, and a 32K data size. Spectra were processed with an exponential multiplication equivalent to 100 Hz of line broadening prior to Fourier transformation, and were referenced to the isotropic peak of the bicelles, which was set to 0 ppm at temperatures between 10 and 15 °C.

¹H NMR diffusion measurements were performed at 499.78 MHz using the STE PFG NMR sequence,³⁸ with square gradient pulses directed along the longitudinal (z) axis and having a constant duration

(5 ms) with variable gradient pulse amplitude. Phase cycling of the radio frequency pulses was employed to remove unwanted echoes.³⁹ The data were acquired using the following typical parameters: a 90° pulse length of 25 μs, a spin echo delay of 10 ms, a stimulated echo delay between 200 and 500 ms, a recycle delay of 1 s, a spectral width of 10 kHz, and a 32K data size. Spectra were processed with an exponential multiplication equivalent to 5 Hz of line broadening prior to Fourier transformation. The gradient strength (typically 300 G cm⁻¹) was calibrated from the known diffusion coefficient of HDO at 25 °C.⁴⁰

In STE PFG NMR diffusion measurements, the resonance intensity I of the species of interest decreases as a function of increasing magnitude of the applied gradient pulses according to eq 2

$$I = I_0 \exp\left[-D(\gamma g \delta)^2 \left(\Delta - \frac{\delta}{3}\right)\right] \quad (2)$$

where D (m² s⁻¹) is the diffusion coefficient, Δ (s) is the experimental diffusion time, γ (rad T⁻¹ s⁻¹) is the relevant magnetogyric ratio, g (T m⁻¹) is the gradient pulse amplitude, and δ (s) is its duration.³⁸ The resonance intensity in the absence of field gradients, I_0 , includes effects arising from longitudinal and transverse relaxation. A semilogarithmic plot of $\ln(I/I_0)$ versus $k = (\gamma g \delta)^2 (\Delta - \delta/3)$ is linear for normal Gaussian diffusion with a slope proportional to the diffusion coefficient.

RESULTS

Morphologies of DMPC/CHAPSO Mixtures from SANS.

Figure 2a,b contains the SANS profiles of 25 wt % DMPC/DHPC and DMPC/CHAPSO mixtures, respectively, as a function of temperature. The SANS patterns and corresponding morphologies of DMPC/DHPC as a function of temperature have been reported previously.^{26,37} They have been interpreted as follows: at temperatures below the gel to liquid-crystalline phase transition temperature of DMPC ($T_M \approx 296$ K), discoidal bicelles (bilayered micelles) are formed. At 25 wt % and with increasing temperature, the bicelles progressively transform into ribbons, then ribbon-meshed lamellae, and eventually multilamellar vesicles (MLVs) (i.e., regularly spaced, stacked onionlike structures that cannot swell once the temperature exceeds ~ 320 K^{22,26,37}). Importantly, the SANS intensity profile from each morphology is distinct. Bicelles yield a SANS profile with a plateau at low q , followed by a decay from q^{-2} to q^{-4} at higher q , whereas the SANS profile from ribbons follows a q^{-1} dependence at low q and a q^{-4} dependence in the high- q regime. In the case of MLVs, a Bragg peak at $q \approx 0.1$ Å⁻¹ is observed and remains invariant upon dilution. The current SANS results for DMPC/DHPC mixtures shown in Figure 2a are consistent with those from previous studies.^{26,37}

SANS profiles for DMPC/CHAPSO shown in Figure 2b demonstrate that CHAPSO-containing neutral bicellar mixtures also form disc structures at temperatures below the T_M of DMPC and MLVs (possibly stacked lamellae) at high temperature ($T \geq 340$ K). As with the DMPC/DHPC mixtures, DMPC/CHAPSO mixtures exhibit a q^{-1} -dependent scattering intensity at low q in the temperature region above 310 K but below the temperature at which the Bragg peak appears, implying the formation of elongated objects. Because of the high C_{1p} , interparticle interactions are not negligible, but an $S(q)$ capable of describing the interactions of such structures is currently not available. As a result, their precise morphology cannot be resolved by fitting the SANS data. However, on the basis of our previous reports of DMPC/DHPC mixtures, these elongated objects are most likely bilayered ribbons or ribbon-meshed lamellae.^{22,26,37}

Despite these similarities, there are subtle differences between the two systems. First, in the case of the DMPC/DHPC system the Bragg peak is observed at 330 K and at 340 K in the case of

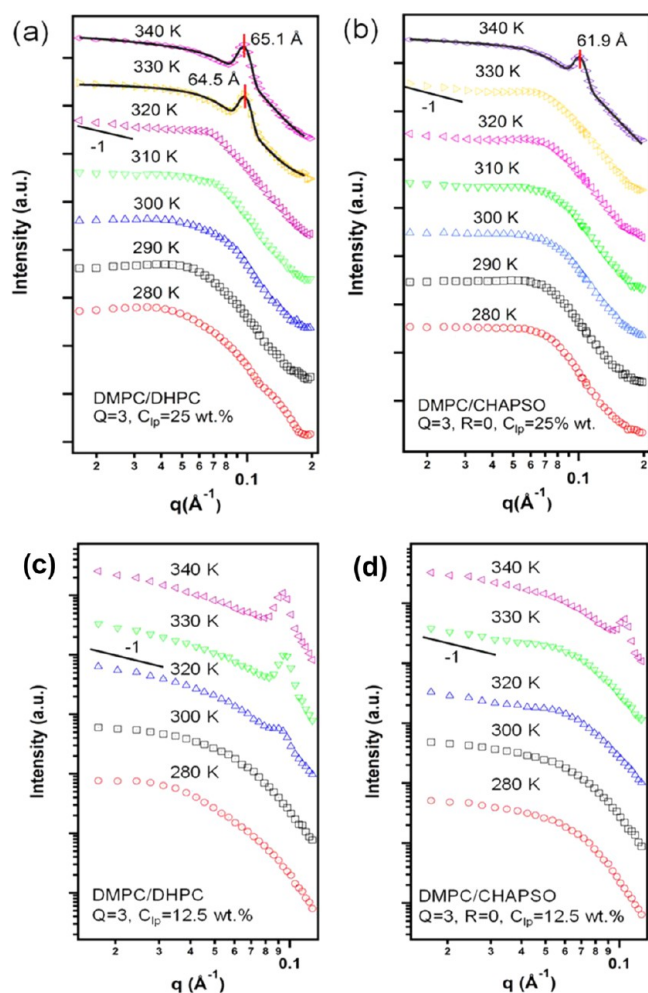


Figure 2. SANS data of (a) DMPC/DHPC and (b) DMPC/CHAPSO mixtures with $C_{ip} = 25$ wt % and (c) DMPC/DHPC and (d) DMPC/CHAPSO mixtures with $C_{ip} = 12.5$ wt % as a function of temperature (between 280 and 340 K in increments of 10 K, as indicated). The curves are the best-fit results for a given morphology as described in the text. The red line indicates the Bragg peak position.

DMPC/CHAPSO, indicating that the DMPC/CHAPSO system is more thermally stable (i.e., it retains the low- T morphology). Second, the d value obtained from the Bragg peak of the DMPC/CHAPSO mixture is slightly smaller (~ 62 Å) than that of the DMPC/DHPC mixture (~ 65 Å). The d value from the DMPC/DHPC system is consistent with previous reports.²¹ An explanation detailing the possible origin of the smaller d -spacing observed in the DMPC/CHAPSO system will be addressed later.

The presence of ribbons, or ribbon-meshed lamellae, is more pronounced in SANS profiles of lower lipid concentration mixtures because the characteristic q^{-1} or approximate q^{-1} dependence at low q values is not as obscured by interparticle interactions. Figure 2c,d compares the temperature dependence of DMPC/DHPC and DMPC/CHAPSO mixtures, respectively, at $C_{ip} = 12.5$ wt %. The q^{-1} dependence of the scattering intensity in the temperature range above the T_M of DMPC is readily evident in both instances. Moreover, the position of the Bragg peak at high temperatures is practically unaffected when the system is diluted from 25 to 2.5 wt %.

Figure 3a,b shows SANS data of DMPC/CHAPSO mixtures at $C_{ip} = 2.5$ and 0.25 wt %, respectively. At $C_{ip} = 2.5$ wt %, the characteristic q^{-1} dependence of the scattering-intensity profile,

indicative of elongated objects, is quite prominent at low q and temperatures just above the T_M of DMPC. Again, the position of the Bragg peak is unaffected by dilution.

The elongated ribbons implied by the SANS data may be well-described by a cylindrical model with an elliptical cross-section, as described in the Supporting Information. Using such a model to fit the SANS data of 2.5 and 0.25 wt % samples at 290 K yielded a ribbon thickness of 52 ± 2 Å and a ribbon length of ~ 700 Å for both samples. The ribbon thickness is slightly larger than the expected DMPC bilayer thickness in the gel phase (~ 48 Å).⁴¹ However, the aspect ratio (major axis/minor axis) of the elliptical cross section obtained from the best fit to the data was smaller for the 2.5 wt % (~ 1.5) sample compared to that for the 0.25 wt % (~ 7.2) sample. However, a polydisperse disc model was also able to fit the 0.25 wt % SANS data equally well and resulted in an apparent lipid bilayer thickness of 53 Å and a disc radius of 213 Å. This model, however, failed to fit the 2.5 wt % SANS data adequately. This suggests that the ribbon structure is most likely the morphology populating the 2.5 wt % sample at 290 K. However, to eliminate any ambiguity regarding the morphology of the 0.25 wt % sample, negatively stained transmission electron microscopy (TEM) was carried out (Figure S2 in the Supporting Information). The micrographs clearly show the presence of discs with sizes similar to those determined from the fits to the SANS data. Hence, we conclude that the morphology of the 0.25 wt % sample at 290 K is discoidal. Increasing the temperature to 310 K for the 2.5 wt % DMPC/CHAPSO mixture resulted in 2-D structures that were possibly large, polydisperse unilamellar vesicles (ULVs) as indicated by the q^{-2} dependence of the SANS intensity (Figure 3a).

The SANS data also indicate that the bicelle/ribbon to MLV (stacked lamellae) transition takes place at 300 K for $C_{ip} = 0.25$ wt % versus 340 K in the case of the higher-lipid-concentration samples. Nevertheless, the Bragg peak position, even at this low lipid concentration, is practically identical to that observed for higher- C_{ip} samples. It should be noted that MLVs consistently appear in DMPC/DHPC mixtures at lower temperatures (330 K for 25 wt % samples and 320 K for 12.5 and 7.5 wt % samples) than for the corresponding DMPC/CHAPSO mixtures, a sign that the bicelles and ribbons made from DMPC/CHAPSO are always more stable than those from DMPC/DHPC. In the case of 0.25 wt % DMPC/DHPC mixtures, morphological changes from bicelles/ribbons to MLVs have previously been observed at temperatures as low as 283 K.²¹

DMPC/DMPG/CHAPSO Morphologies: Mixtures at Higher Concentrations (SANS). It is known that adding a small amount of negatively charged phospholipid DMPG to a DMPC/DHPC bicellar mixture can result in drastic changes to the structural phase diagram.⁴² One of the most significant differences is the absence of MLVs at high temperatures due to the presence of strong Coulombic repulsion between lamellae. Instead, mixtures with DMPG form perforated lamellae whose d spacing varies with C_{ip} .²¹ Here, DMPC/DMPG/CHAPSO mixtures with two different molar ratios of DMPG, namely, $R = 0.01$ and 0.10, have been examined. These experiments were performed in order to compare the effects of surface charge in CHAPSO-containing mixtures with those known to occur in DHPC-containing mixtures.

Figure 4a,b shows SANS data of 25 wt % DMPC/DMPG/CHAPSO mixtures with $R = 0.01$ and 0.10, respectively. In the case of the $R = 0.10$ mixture, a Bragg peak corresponding to the lamellar d spacing appears at 310 K and above. In contrast, the R

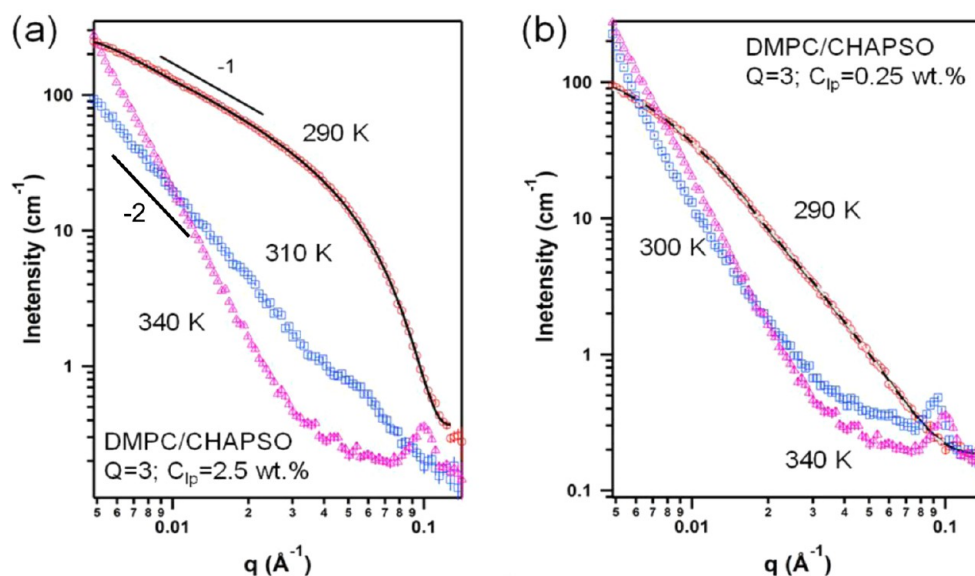


Figure 3. SANS data of DMPC/CHAPSO mixtures with C_{lp} values of (a) 2.5 and (b) 0.25 wt %. The solid lines are the best fits using the elliptical cross-section cylindrical model, representing bilayered ribbons. In plot b, the dashed gray line is the best fit of the polydisperse discoidal model, representing discoidal bicelles, which in this case overlaps with the best fit of the elliptical cross-section cylindrical model (solid black line).

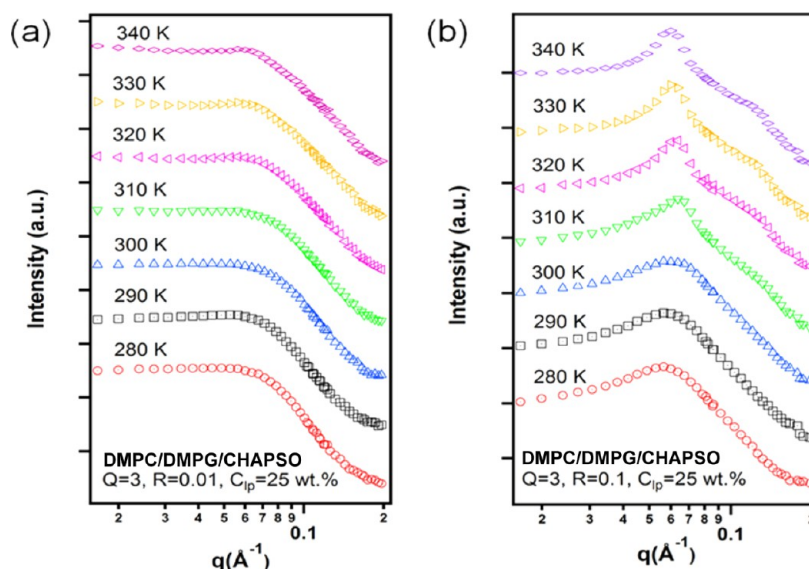


Figure 4. SANS data of DMPC/DMPG/CHAPSO mixtures at $C_{lp} = 25$ wt % with (a) $R = 0.01$ and (b) $R = 0.10$ at temperatures between 280 and 340 K, in increments of 10 K.

$= 0.01$ sample shows no such transition over the temperature range studied. The difference between the two samples suggests that the lower surface charge of the $R = 0.01$ sample leads to a less-well-defined positional correlation between bilayers. Nevertheless, it seems that even a small surface charge ($R = 0.01$) is sufficient to prevent MLVs from forming (i.e., no Bragg peak at $q \approx 0.1 \text{ \AA}^{-1}$).

Figure 5a,b shows SANS profiles at 330 and 340 K, respectively, for $R = 0.01$ DMPC/DMPG/CHAPSO mixtures as a function of lipid concentration: $C_{lp} = 25, 12.5$, and 7.5 wt %. With decreasing lipid concentration, lamellar Bragg peaks are clearly visible and higher-order peaks are starting to appear. The inset to the figure shows the changes in d spacing, as determined from the first-order Bragg peak, as a function of decreasing lipid concentration. This behavior is very different from the invariant peak position of MLVs formed by zwitterionic systems. Figure

5c,d shows SANS profiles at 330 and 340 K, respectively, for $R = 0.10$ DMPC/DMPG/CHAPSO mixtures as a function of lipid concentration: $C_{lp} = 25, 12.5$, and 7.5 wt %. As with the $R = 0.01$ sample, higher-order Bragg peaks begin to appear, and the d spacing increases with decreasing lipid concentration.

Table 1 summarizes the d spacings measured at 330 and 340 K from the SANS profiles shown in Figure 5. All d spacings were obtained using the q_{max} of the first-order Bragg peaks. The key findings can be summarized as follows: (i) compared to $R = 0.10$ samples, d spacings are generally larger for $R = 0.01$ samples; (ii) d spacings at 340 K are generally greater than those at 330 K; (iii) d spacings are inversely related to lipid concentration; and (iv) differences in d spacing between the different samples diminish with increasing lipid concentration, whereby at $C_{lp} = 25$ wt % d spacings are found to be clustered at just over 100 \AA .

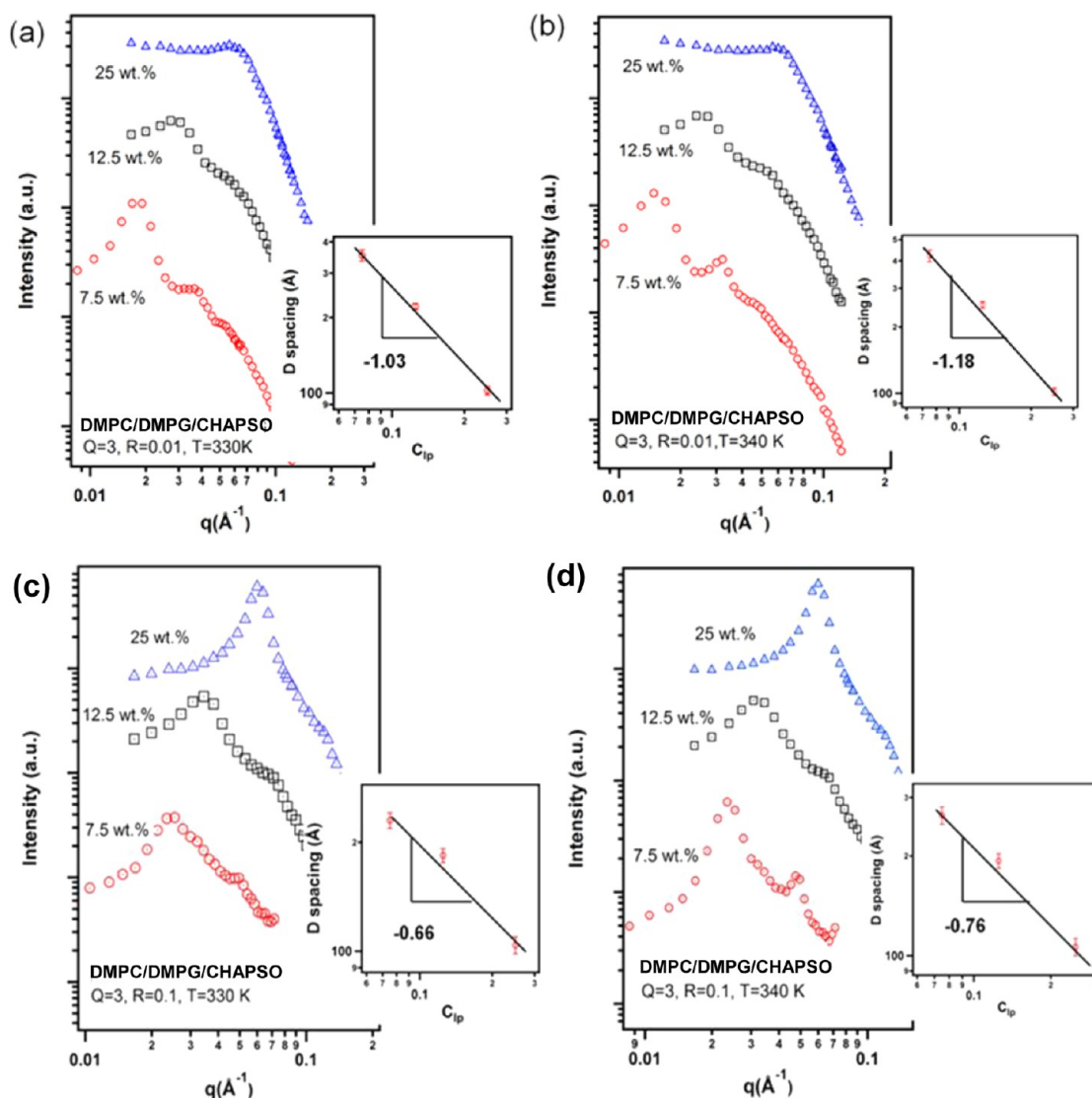


Figure 5. SANS data of high- C_{ip} (25, 12.5, and 7.5 wt %) DMPC/DMPG/CHAPSO ($R = 0.01$) mixtures at (a) $T = 330$ K and (b) 340 K and DMPC/DMPG/CHAPSO ($R = 0.10$) mixtures at (c) $T = 330$ K and (d) 340 K. The insets illustrate the d spacing as a function of C_{ip} .

Table 1. Summary of Lamellar d Spacings of DMPC/DMPG/CHAPSO at Different Concentrations

	d spacing (Å) ($R = 0.01$)		d spacing (Å) ($R = 0.10$)	
	330 K	340 K	330 K	340 K
7.5%	353.4	422.2	230.1	265.1
12.5%	220.9	251.8	183.9	193.1
25%	102.1	101.8	103.9	106.2

In the case of perfect, nonperforated, and swellable lamellae, the d spacing is expected to change linearly upon dilution (i.e., $d \propto C_{ip}^{-1}$). This type of swelling is clearly evident in $R = 0.01$ mixtures at both temperatures (insets of Figure 5a,b). This same behavior was observed in DMPC/DMPG/DHPC mixtures.²¹ In the case of $R = 0.10$, d is proportional to $C_{ip}^{-0.66}$ or $C_{ip}^{-0.76}$, deviating from the 1-D swelling behavior (insets of Figure 5a,b). It should be noted that the morphological transformation between high and low T in the high- C_{ip} samples is completely reversible (Figure S3 in Supporting Information).

DMPC/DMPG/CHAPSO Morphologies: Mixtures at Lower Concentrations (SANS). Figure 6a,b shows SANS results of low- C_{ip} DMPC/DMPG/CHAPSO mixtures at $R =$

0.01 and 0.10, respectively (0.25 and 2.5 wt %), and at $T = 290$ and 340 K. In the case of the $R = 0.01$ mixture (Figure 6a) at 290 K and 0.25 wt %, bicelles are observed and fits to the data result in a bilayer thickness of ~ 51 Å. At 2.5 wt % and 290 K, the profile of the $R = 0.01$ sample is indicative of ribbons, and fits to the data yield a similar bilayer thickness (~ 51 Å) to that of bicelles in the 0.25 wt % sample. At 340 K, SANS data of both 0.25 and 2.5 wt % samples with $R = 0.01$ contain intensity oscillations as a function of q , indicating the presence of uniformly sized ULVs. This morphology was modeled using a polydisperse spherical shell model (Supporting Information). The best fit of the data results in a shell thickness of ~ 42 Å and a vesicular radius, R_v , that increases with increasing lipid concentration from 174 Å ($C_{ip} = 0.25$ wt %) to 469 Å ($C_{ip} = 2.5$ wt %), consistent with the trend reported in the DMPC/DMPG/DHPC system.^{21,43} A smaller lipid bilayer thickness with increased temperature can be attributed to the melting of the DMPC acyl chains and is consistent with what is seen in pure DMPC ULVs.

In the case of the highly charged $R = 0.10$ mixture (Figure 6b) at $C_{ip} = 0.25$ wt %, only the polydisperse disc model is able to fit the SANS data at both $T = 290$ and 340 K, consistent with results

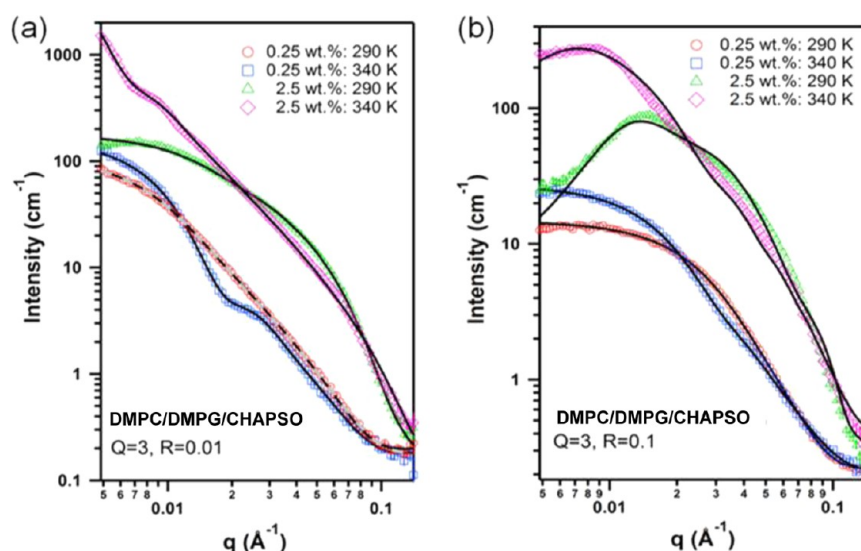


Figure 6. SANS data of DMPC/DMPG/CHAPSO mixtures at $C_p = 0.25$ and 2.5 wt % with (a) $R = 0.01$ and (b) $R = 0.10$ at different temperatures. For the 0.25 wt %, $R = 0.01$, and $T = 290$ K case in plot a, both the elliptical cross-section cylindrical model (ribbons) (solid black curve) and the discoidal bicelle model (dashed gray curve) adequately fit the SANS data. At 340 K, however, the elliptical cross-section cylindrical model provides the best fit. For the 2.5 wt %, $R = 0.01$ sample in plot a, the elliptical cross-section model fits the data better at 290 K, whereas the polydisperse spherical shell model (ULVs) was best at 340 K. For the $R = 0.10$ cases shown in plot b, all data were best fit using the discoidal bicelle model with a structure factor for higher C_p samples.

previously reported using the DMPC/DMPG/DHPC system,²¹ where at low C_p the disc morphology was stable from 283 to 318 K. The disc radius increases from 70 Å at 290 K, to 123 Å at 340 K. At $C_p = 2.5$ wt %, $S(q)$ is no longer negligible, as significant pseudo-Bragg peaks begin to crop up, corresponding to the interparticle spacing, and shift from high- q to low- q values upon heating (i.e., increased spacing), implicating bicelle growth if one assumes the conservation of mass. By using the polydisperse disc model with the Hayter–Penfold structure factor⁴⁴ we found that the best-fit disc radius increases from 68 Å at 290 K, to 154 Å at 340 K.

Magnetic Alignment of DMPC/DMPG/CHAPSO Mixtures (^{31}P NMR). Under certain conditions, bicellar mixtures align in a magnetic field, a feature that has contributed considerably to their popularity in NMR studies. ^{31}P NMR is a useful tool with which the quality of bicellar magnetic alignment can be accessed,²⁵ and has been used here to compare the thermal stability of magnetic alignment in DMPC/CHAPSO, DMPC/DMPG/CHAPSO, and DMPC/DHPC mixtures, all having $Q = 3$. All were examined at $C_p = 25$ wt % because at low C_p magnetic alignment can be problematic regardless of composition.

Figure 7a compares the ^{31}P NMR spectra of DMPC/DHPC, DMPC/CHAPSO, and DMPC/DMPG/CHAPSO mixtures at $C_p = 25$ wt % as a function of temperature. For the DMPC/DHPC mixture at 298 K, a temperature close to the T_M of DMPC, the spectrum consists of a broad powder pattern line shape with a width on the order of 45 ppm, indicating a powder distribution of DMPC orientations⁴⁵ and demonstrating that magnetic alignment has not yet occurred. The bicellar assemblies experience slow reorientational motions, which are defined by the inverse of the powder pattern width of 45 ppm. The observed narrow resonance at the isotropic frequency (0 ppm) is due to DHPC, which occupies highly curved edge regions and hence experiences nearly isotropic motional averaging. At a temperature just above 298 K, the broad DMPC powder pattern disappears and is replaced by a narrow resonance at a frequency

of roughly -12 ppm (e.g., 308 K in Figure 7a), indicative of a uniform alignment of the bicellar aggregates with their bilayer normal perpendicular to the magnetic field. This so-called negative magnetic alignment arises spontaneously from the negative magnetic susceptibility anisotropy of the bicellar assembly.⁴⁶ The second and smaller resonance at roughly -5 ppm is assigned to DHPC. The fact that DHPC's ^{31}P NMR resonance no longer appears at the isotropic frequency indicates that DHPC undergoes fast exchange between edge and planar regions, per the mixed bicelle model.²⁶ At 318 K, as shown in Figure 7, a third resonance appears at -13.8 ppm, similar to that observed by Triba et al.²⁶ that was attributed to deformed vesicles, undoubtedly corresponding to a more highly ordered population of lipids. It appears at a temperature that correlates closely with that at which the Bragg peak appears in the comparable SANS profile in Figure 2a, thus indicating an MLV (or stacked lamellar) structure.

For the DMPC/CHAPSO mixture at 298 K, a powder pattern spectrum was not observed: rather, a broad featureless spectrum was obtained, centered at 0 ppm. This is indicative of assemblies undergoing overall reorientational motions at a rate intermediate to the inverse of the powder spectrum width of 45 ppm. This difference versus the DMPC/DHPC mixture may be due to the same structural effects that produce the different viscosity temperature minimum of 4 °C for DMPC/DHPC versus 15 °C for the DMPC/CHAPSO mixture.

At a temperature of 308 K, the DMPC/CHAPSO mixture yields a single narrow resonance at a frequency indicative of a highly negatively aligned DMPC population. Note that CHAPSO contains no phosphorus atoms, thus yielding no ^{31}P NMR resonance. At 318 K, in contrast to the corresponding DMPC/DHPC mixture where the bicelle morphology appears to have been altered significantly, the ^{31}P NMR spectrum of the DMPC/CHAPSO mixture is essentially identical to that obtained at 308 K. Eventually, at temperatures exceeding 330 K the spectrum splits into two resonances, the dominant one at the isotropic frequency and the other at -13.3 ppm. At such

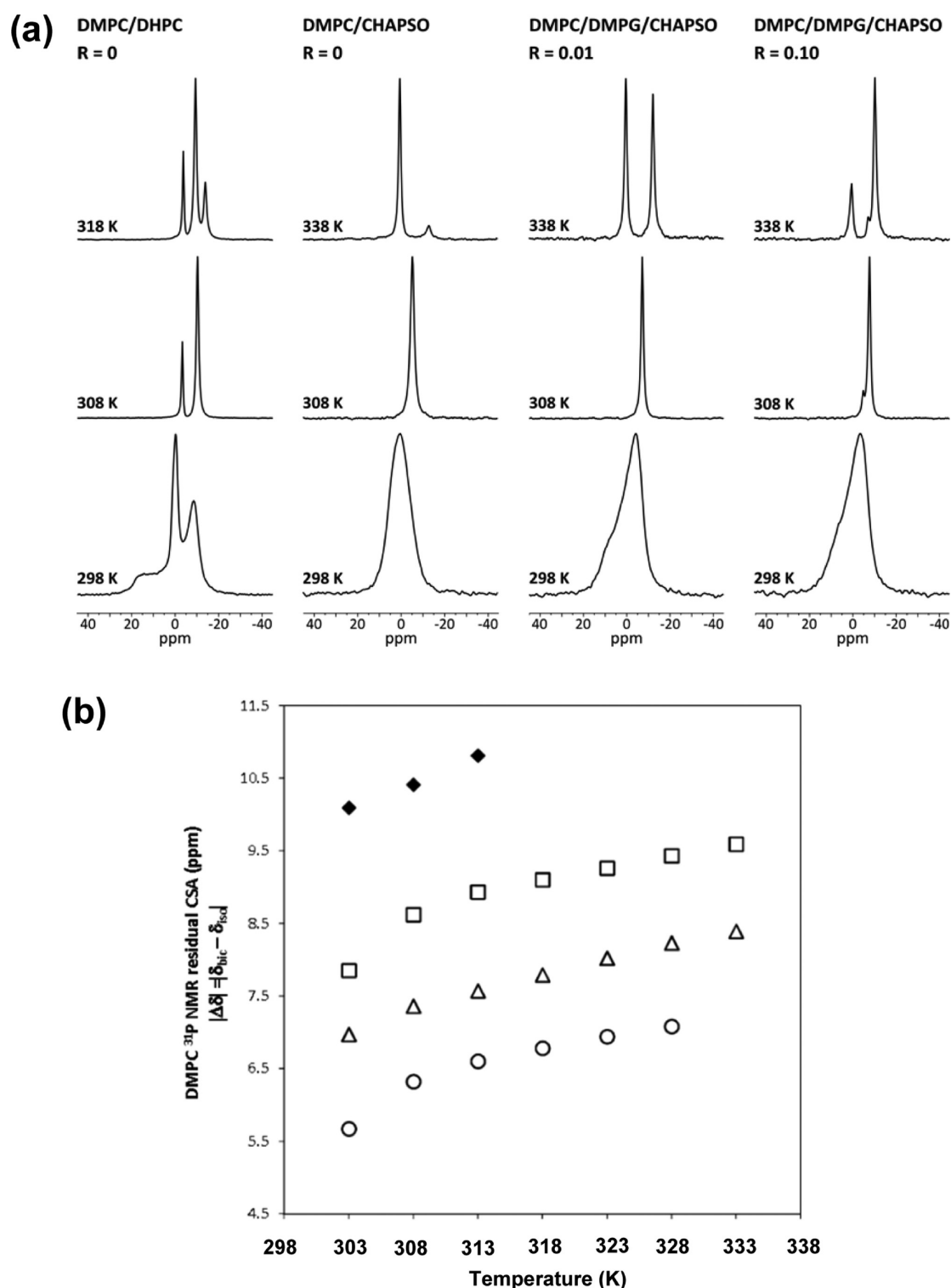


Figure 7. (a) ^{31}P NMR spectra of DMPC/DHPC (left-hand column) and various DMPC/DMPG/CHAPSO samples, as indicated, with $Q = 3$ and $C_{\text{lp}} = 25$ wt % at the indicated temperatures and (b), ^{31}P NMR residual chemical shift anisotropy spectra of DMPC as a function of temperature of different negatively magnetically aligned, $Q = 3$, $C_{\text{lp}} = 25$ wt % mixtures: DMPC/DHPC (♦); DMPC/CHAPSO (○); DMPC/DMPG/CHAPSO, $R = 0.01$ (△); and DMPC/DMPG/CHAPSO, $R = 0.10$ (□).

elevated temperatures, there are therefore two populations of DMPC: one undergoing isotropic motions and one corresponding to the deformed vesicles. This temperature also corresponds to the appearance of the Bragg peak in SANS profiles of DMPC/CHAPSO at 340 K (Figure 2b). Note that undeformed MLVs would yield a powder pattern line shape similar to that seen at

298 K for DMPC/DHPC rather than the narrow resonance at -13.3 ppm, indicative of continued magnetic alignment. To reconcile the SANS and ^{31}P NMR results, one may invoke the presence of a highly ordered, closely stacked lamellar domain. Note that this lamellar structure interpreted as MLVs in SANS data may contain defects stabilized by DHPC or CHAPSO and

are thus presumably magnetically alignable. We postulate that at such elevated temperatures CHAPSO may separate from DMPC, forming a nonalignable CHAPSO-rich phase coexisting with DMPC-rich lamellae.

The ^{31}P NMR spectra indicated comparable behavior in all DMPC/DMPG/CHAPSO mixtures. Note that for the $R = 0.10$ case, the ^{31}P NMR resonance of DMPG becomes visible as a shoulder on the DMPC resonance. At approximately 333 K, separation into two populations is again apparent, one exhibiting an isotropic frequency and the other apparently more ordered. With increasing DMPG content from $R = 0$ to 0.01 to 0.10, the fractional population exhibiting an isotropic resonance declines precipitously. This too is in fundamental agreement with the SANS results, indicating greater thermal stability of the alignable phase in the presence of surface charge as a result of the inclusion of DMPG. Overall, these ^{31}P NMR spectra demonstrate that the DMPC/CHAPSO and DMPC/DMPG/CHAPSO mixtures have a wider temperature range over which a homogeneous magnetically alignable phase is observed than found for DMPC/DHPC mixtures. Thus, CHAPSO-containing systems exhibited a significantly greater thermal stability of morphology than the DHPC-containing ones.

The quality of the magnetic alignment in these bicelle mixtures can be examined in greater detail via a comparison of the residual ^{31}P NMR chemical shift anisotropy $\Delta\delta = |\delta_{\text{bic}} - \delta_{\text{iso}}|$ exhibited under particular circumstances, where δ_{bic} is the observed DMPC chemical shift for a particular bicellar composition at a given temperature, and δ_{iso} is the isotropic chemical shift. Figure 7b illustrates such a comparison as a function of T for the different mixtures of interest here. In each instance, $\Delta\delta$ increased with increasing temperature. Although this observation seems contradictory to the notion that strong thermal fluctuations should decrease the ordering of the lamellae, it can be understood to arise from the formation of larger discs, ribbons, or lamellae upon the coalescence of smaller aggregates. For DMPC/DHPC mixtures, this coalescence is driven by the increased miscibility of DHPC with DMPC, with increasing temperature, as suggested elsewhere,^{26,27,47} which decreases the amount of DHPC available to populate edge regions. ^{31}P NMR cannot directly monitor CHAPSO in bicelles, but the fact that similar behavior is observed with both DHPC- and CHAPSO-containing mixtures suggests a similar increase in CHAPSO miscibility with DMPC with increased temperature. The higher ordering for DHPC- versus CHAPSO-containing DMPC mixtures evident in Figure 7b has been observed previously by Sanders et al.^{1,29} and is believed to arise from the greater efficiency with which CHAPSO masks edge regions, thus allowing more “edge” per mole, hence resulting in smaller aggregates (or lamellae containing more defects) having lower orientational order.

At any specific temperature, $\Delta\delta$ of the DMPC/DMPG/CHAPSO mixture increases with increased DMPG content (from $R = 0$ to 0.01 to 0.10). This may be understood to arise from a progressive “stiffening” of the bilayers with increasing DMPG, as the associated surface charge dampens thermal undulations within and between the membranes, thereby enhancing their ordering.^{48–50} Nevertheless, even at 10 mol % DMPG (i.e., $R = 0.10$) the DMPC/DMPG/CHAPSO mixture exhibits a smaller $\Delta\delta$ than corresponding DMPC/DHPC mixtures (i.e., lacking DMPG entirely) at the same temperature and lipid concentration.

^{31}P NMR provides a useful overview of the phase homogeneity, magnetic alignment, and orientational order

present in bicellar mixtures. However, certain morphologies, such as ribbons and perforated lamellae, provide essentially identical ^{31}P NMR spectra. Diffusion NMR, however, may differentiate such details,⁵¹ and these studies are presented next.

Water and PEG Diffusion in Interbicellar Spaces. ^1H PFG STE NMR diffusion studies were undertaken to compare CHAPSO-containing and DHPC-containing systems, where PEG-1000 was incorporated as a diffusion probe of the bicellar interstitial space. In particular, it was of interest to investigate whether it was possible to observe the so-called ribbon morphology, where nonexponential and time-dependent diffusive decays may be observed.³⁷

Figure 8a shows a series of ^1H PFG STE NMR spectra for DMPC/DMPG/CHAPSO mixtures ($R = 0.10$ and $C_{\text{pl}} = 25$ wt

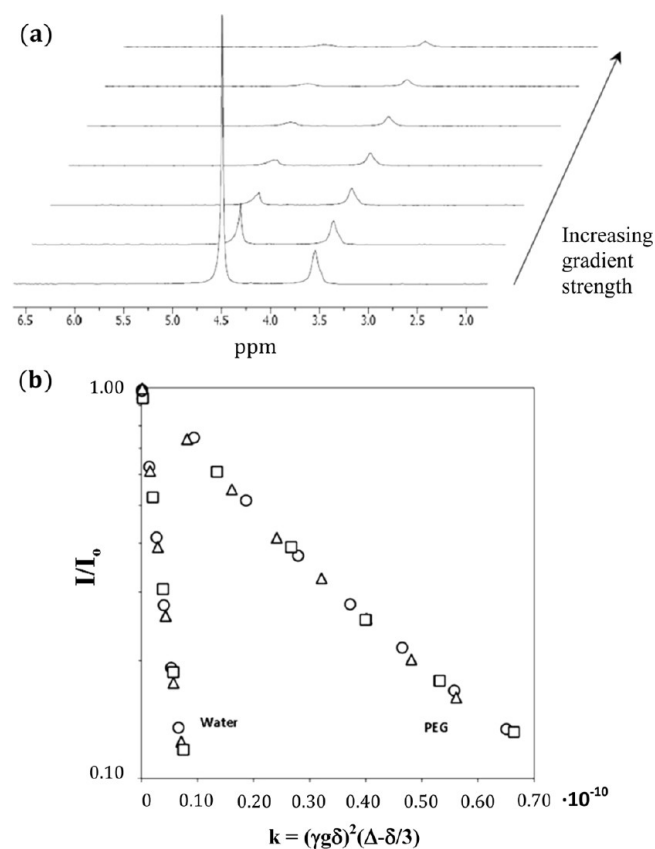


Figure 8. (a) ^1H PFG STE NMR spectra of negatively magnetically aligned DMPC/DMPG/CHAPSO, $R = 0.10$, $C_{\text{pl}} = 25$ wt % mixtures at 333 K as a function of increasing gradient pulse amplitude. The only resonances visible are those of water (4.3 ppm) and the ethylene oxide units of PEG-1000 (3.4 ppm). The intensity decay reflects center-of-mass diffusion. (b) Semilogarithmic plots of the normalized intensity of the water resonance and PEG-1000 resonance from ^1H PFG STE NMR spectra of negatively magnetically aligned DMPC/DMPG/CHAPSO, $R = 0.10$, $C_{\text{pl}} = 25$ wt % mixtures at 333 K as a function of the experimental factor $k = (\gamma\delta)^2(\Delta - \delta/3)/10^{-10}$ for different experimental diffusion times: 50 ms (\circ), 100 ms (Δ), and 200 ms (\square). As per eq 2, the diffusion coefficient is extracted from the slope in such a plot.

%) acquired at 333 K, at which negative magnetic alignment is still present. The spectra contain only two resonances, one at 4.3 ppm corresponding to water and the other at 3.4 ppm arising from the ethylene oxide protons of PEG-1000. Other possible resonances are not visible because of residual dipolar interactions, which shorten their transverse relaxation times

relative to the delays in the PFG STE pulse sequence. The spectral series in Figure 8a was acquired with increasing gradient amplitude g so that diffusion leads to a progressive decrease in signal intensity across the series. (Obviously, water diffuses more quickly than does PEG-1000.) The diffusion coefficient may be extracted from the intensity decay as per eq 2.

For the case of a molecule diffusing within the interstitial spaces between magnetically aligned lamellae, the diffusion coefficient will be anisotropic in two directions: (1) perpendicular to the bilayer normal and characterized by a diffusion coefficient D_{\perp} , and (2) parallel to the bilayer normal and characterized by a diffusion coefficient D_{\parallel} , which is obstructed by the intervening surface of the adjacent lamellae. The experimentally measured diffusion coefficient depends on the orientation of the applied field gradients. For the case of field gradients applied along the z direction (i.e., parallel to the direction of the main magnetic field), as in the present case, the measured diffusion coefficient, D_{zz} , is related to the diffusion tensor components in the magnetically aligned bicelle reference frame via eq 3

$$D_{zz} = D_{\perp} \sin^2 \theta + D_{\parallel} \cos^2 \theta \quad (3)$$

where θ is the angle between the bilayer normal and the direction of the applied field gradients.^{52,53} For these negatively magnetically aligned bilayers ($\theta = 90^\circ$), the measured diffusion coefficient is D_{\perp} .

Figure 8b shows representative diffusion decays obtained via ^1H PFG STE NMR measurements on negatively magnetically aligned DMPC/DMPG/CHAPSO mixtures ($R = 0.10$) at 333 K. Intensity decays for water and for PEG-1000 are plotted for different diffusion times Δ . All exhibit monoexponential behavior and diffusion time independence, indicative of normal Gaussian, nonrestricted diffusion. Similar behavior was obtained for all bicellar compositions investigated here within the range of temperatures over which stable magnetic alignment was observed. From the slope one extracts the particular diffusion coefficient. For water, the diffusion coefficient was on the order of $3.0 \times 10^{-9} \text{ m}^2 \text{ s}^{-1}$, which is roughly 30% of that of bulk water at the same temperature. This reduction is due, in large measure, to the population of lipid-bilayer-bound water. The PEG-1000 diffusion coefficient was found to equal $3.2 \times 10^{-10} \text{ m}^2 \text{ s}^{-1}$, representing an approximately 60% reduction in the diffusion coefficient relative to PEG-1000 free in solution at the same temperature. This reduction can be attributed to the confinement of PEG-1000 in the channels formed by the magnetically aligned membranes, further verifying the lamellar structure.⁵⁴

Given the diffusion coefficient, D , and the experimental diffusion time $t = \Delta$, one may calculate the root-mean-square (rms) displacement undergone by the diffusant during the course of the measurement as per eq 4.

$$\langle r^2 \rangle^{1/2} = (4Dt)^{1/2} \quad (4)$$

For water, the rms displacements fall in the range between 17 and 50 μm for lower temperature—shorter diffusion time measurements ($T = 303 \text{ K}$, $\Delta = 50 \text{ ms}$) versus higher temperature—longer diffusion time measurements ($T = 333 \text{ K}$, $\Delta = 200 \text{ ms}$). For PEG-1000, the same range of experimental conditions yields rms displacements of between 5 and 15 μm . The PFG NMR diffusion decays demonstrate, therefore, that these diffusants experience unrestricted normal diffusion on these length scales.

Figure 9 illustrates an Arrhenius plot of the T dependence of both water and PEG-1000 diffusion coefficients in different

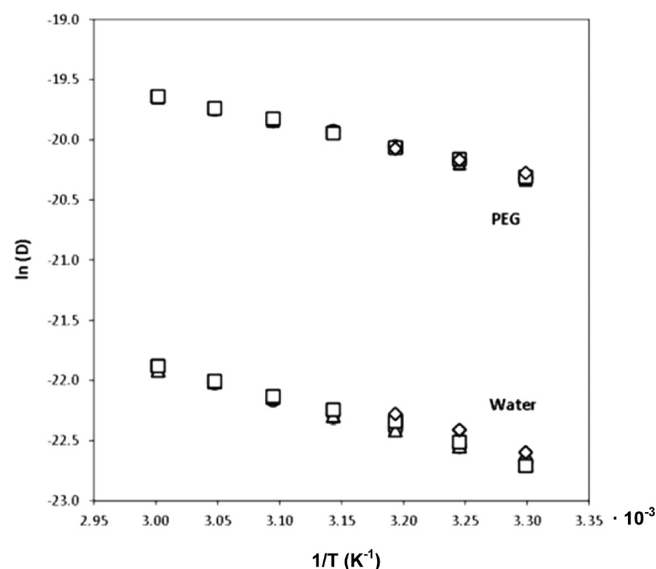


Figure 9. Arrhenius plot of the natural logarithm of the diffusion coefficients of water and PEG-1000 vs reciprocal temperature for various negatively magnetically aligned $Q = 3$, $C_{\text{lp}} = 25 \text{ wt } \%$ mixtures: DMPC/DHPC (\diamond); DMPC/CHAPSO (\circ); DMPC/DHPC/CHAPSO, $R = 0.01$ (\triangle); and DMPC/DMPG/CHAPSO, $R = 0.10$ (\square).

bicelle systems. The comparison demonstrates little difference in the diffusion behavior across various bicelle compositions for either diffusant. The activation energies for diffusion are listed in Table 2. For water, the activation energies are similar to the literature value for pure water (18.8 kJ/mol between 15 and 45 $^\circ\text{C}$).⁴⁰ For PEG-1000, the activation energies were significantly higher than that of free PEG-1000 in aqueous solution, as expected given its size relative to the confinement dimensions of the interlamellar spacings.⁵⁴

DISCUSSION

Relative Morphological Stability of DHPC- and CHAPSO-Containing Mixtures. Both SANS and ^{31}P NMR results demonstrate that bicellar mixtures destabilize at elevated temperature. In SANS, this is manifested by the appearance of a Bragg scattering peak, whereas in ^{31}P NMR it is revealed by the appearance of additional resonances at or near the isotropic resonance. These results point to a separation of amphiphile populations into detergent-rich and detergent-depleted domains at sufficiently elevated temperatures. The detergent-rich domains give rise to an isotropic ^{31}P NMR resonance. The detergent-depleted domains, containing a more planar structure, give rise to a Bragg scattering peak in SANS data (interpreted as MLVs) and increased orientational order in ^{31}P NMR spectra. Similar temperature-dependent ^{31}P NMR spectra have been reported previously by Triba et al.²⁶ for analogous DMPC/DHPC mixtures, and by Sanders and Prestegard²⁹ for analogous DMPC/CHAPSO mixtures. Likewise, DMPC/Na cholate mixtures around $Q = 3$ exhibit similar instabilities at elevated temperatures as evident in ^{31}P NMR spectra.⁵⁵ Here we observe that the upper temperature limit of structural stability is higher in CHAPSO- versus DHPC-containing mixtures at all C_{lp} values. Before addressing the likely origin of these observations and the greater thermal stability of CHAPSO- versus DHPC-containing bicellar mixtures, it is useful to eliminate some particular possibilities from the discussion.

Table 2. Activation Energies for Water and PEG-1000 Diffusion in Various Negatively Magnetically Aligned Bicelles

short-chain lipid		CHAPSO	CHAPSO	CHAPSO	DHPC	
R = DMPG/DMPC		0	0.01	0.10	0	control (aq sol)
E_{ACT} (kJ/mol)	water	18.8 ± 1.7	19.1 ± 1.6	18.6 ± 1.5	15.9 ± 5.5	19.7 ± 1.2
	PEG-1000	21.6 ± 1.2	22.2 ± 1.5	22.3 ± 1.4	25.0 ± 4.5	20.0 ± 2.4

First, it is unlikely that there is a significant pool of unbound detergent present in solution for either DHPC or CHAPSO. The strength of detergent partitioning into fluid lipid bilayers, as quantified by the partition coefficient, K , scales roughly inversely with the detergent's critical micellation concentration (cmc) (i.e., $K \propto 1/\text{CMC}$).⁵⁶ Literature values for the CMC of CHAPSO (8 mM)⁵⁷ and DHPC (15 mM)⁵⁸ suggest then the possibility that CHAPSO has higher partitioning into lipid bilayers. However, the mole fraction of bilayer-bound detergent is⁵⁶

$$X_b^d = \frac{K[L]}{1 + K[L]} \quad (5)$$

where $[L]$ is the concentration of bilayer lipids. Thus, at a lipid concentration corresponding to $C_{lp} = 25$ wt %, effectively both detergents, whether DHPC or CHAPSO, would be virtually completely bilayer-bound, within a few percent, regardless of their different partition coefficients.

Second, it seems unlikely that one is observing solubilization of the bilayer region by the detergent (i.e., DHPC or CHAPSO), as this is commonly understood. In the widely accepted three-stage model of lipid solubilization by detergents (reviews in Lichtenberg et al.⁵⁹), the lipid phase is able to accommodate detergent up to some saturation detergent/lipid mole ratio, R_d^{sat} , without the disruption of the bilayer structure. Additional detergent induces a mixed phase consisting of a detergent-saturated lipid lamellar phase coexisting with a lipid-saturated detergent micellar phase. Eventually, above a detergent/lipid mole ratio of R_d^{sol} , additional detergent produces a single mixed detergent–lipid micellar phase, at which point the lipid bilayer is solubilized. At $Q = 3$, both DHPC and CHAPSO remain well below the saturation level R_d^{sat} at which a micellar phase would first be expected to appear. Moreover, both R_d^{sat} and R_d^{sol} generally increase with increasing T (i.e., the lipid bilayer accommodating more detergent before R_d^{sat}). Although nonintuitive, this is understood to arise from differential effects of temperature on the spontaneous curvature of the lipid versus the detergent.⁵⁹ The expansion of the hydrocarbon portion of the long-chain lipids with increased T makes their spontaneous curvature more negative so that more detergent is required to solubilize the bilayer. Simultaneously, the detergent's spontaneous curvature becomes less positive, resulting in a less conical detergent that is thus less effective in solubilization. Hence, different bilayer solubilization by DHPC versus CHAPSO with increased T does not appear to offer an explanation for the observed differences in thermal stability in structure between these two systems.

A phenomenon observed in certain detergent–lipid mixtures is that a micelle-to-lamella transition may be induced thermally at a constant detergent-to-lipid ratio.⁶⁰ Specifically, a detergent–lipid dispersion in the purely micellar phase can be converted to the coexisting lamellae plus micelles phase simply by raising the temperature. The effect is completely reversible upon lowering the temperature and is attributed to a significant decrease in the detergent's cmc with increased T . This is clearly opposite to the effects observed here at higher T , where increasing T drives a separation into coexisting micellelike and lamellar structures for both DHPC- and CHAPSO-containing mixtures. Furthermore,

dynamic light scattering (DLS) measurements on CHAPSO and DHPC, as part of our investigations (Supporting Information), confirm the CMCs of CHAPSO and DHPC, as reported in the literature,⁵⁸ and demonstrate no significant temperature dependence of either's CMC over the relevant temperature range.

The many useful properties of bicellar mixtures depend on the degree of nonideal mixing of the detergent with the long chain lipid. This limited miscibility means that “curvaphilic” detergents with a high positive spontaneous curvature tend to occupy edge regions whereas “curvophobic” long-chain lipids with a slightly negative spontaneous curvature prefer planar regions.⁵⁸ In the gel phase, this miscibility is at its lowest, leading to the greatest line integral of edge regions, producing small discoidal assemblies. Above the gel to liquid-crystalline phase-transition temperature, the increased miscibility with increased T progressively diminishes the DHPC available to cover edge regions, thus decreasing the line integral of edge regions promoting the fusion into larger assemblies (ribbons or perforated lamellae). Larger assemblies exhibit greater orientational order, as manifest in the increasing ^{31}P NMR chemical shift anisotropy with increasing temperature shown in Figure 7. The fact that CHAPSO-containing mixtures exhibit the same trend suggests a similarly increased miscibility with increased T . Because CHAPSO does not have a phosphorus atom, the current ^{31}P NMR measurements cannot address this question. However, another approach, such as ^2H NMR of deuterium-labeled CHAPSO, might be able to do so.

The general correlation between the size of bicellar assemblies and their orientational order, as manifested in the ^{31}P NMR residual chemical shift anisotropy,¹ suggests that CHAPSO-containing assemblies are significantly smaller or contain more defects than DHPC-containing assemblies (i.e., the line integral of edge regions per mole of detergent is greater for CHAPSO). An inspection of their different chemical structures, as shown in Figure 1, shows that CHAPSO's amphiphilicity arises from the presence of opposing hydrophobic and polar faces rather than from the hydrophobic tail and polar headgroup arrangement in DHPC. As proposed in the earliest studies of CHAPSO-containing bicelles,²⁹ CHAPSO may lie flat on a hydrophobic surface, thereby masking a greater hydrophobic surface area per molecule than DHPC, which is conical and assembles into a hemispherical coating. Note that it is not necessary to postulate differential bilayer miscibility for DHPC versus CHAPSO in order to explain qualitatively the different behaviors of the assemblies formed upon mixing with DMPC, although such a differential miscibility may well exist.

As to the high-temperature instability observed with DHPC, Triba et al.²⁶ observed a similar evolution in their ^{31}P NMR spectra. The upfield resonance was ascribed to vesicles coexisting with DHPC-enriched perforated lamellae. These authors argue that the progressive movement of DHPC into the bilayer with increasing T eventually forces vesiculation as the line tension energy exceeds the bending energy. With CHAPSO, the picture is somewhat different at high temperature, aside from a higher thermal stability. As has been reported previously,²⁹ CHAPSO-containing mixtures at such temperatures are clearly divided into

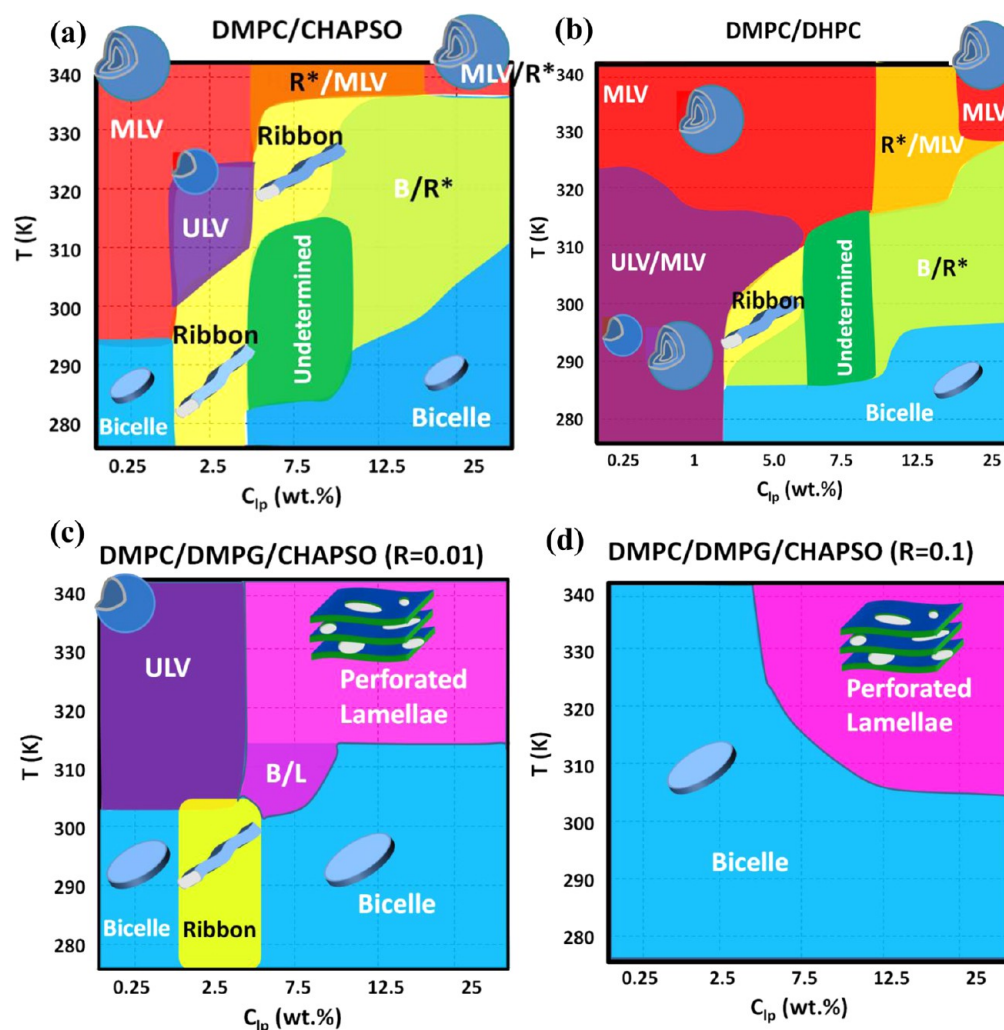


Figure 10. Spontaneous forming structures (temperature vs. lipid concentrations) of (a) DMPC/CHAPSO, (b) DMPC/DHPC, (c) DMPC/CHAPSO/DMPG ($R = 0.01$), and (d) DMPC/CHAPSO/DMPG ($R = 0.10$) mixtures. R^* represents a possible mixture of ribbons and ribbon-meshed lamellae. The regions with possible coexisting structures are shown using combined colors (e.g., orange represents a mixture of R^* (yellow) and MLV (red), light green represents a mixture of bicelle (blue) and R^* (yellow), and dark purple represents a mixture of ULV (purple) and MLV (red)).

two DMPC-containing populations: one experiencing isotropic motion, being small in size, and the other experiencing anisotropic motion, being large in size, which remains magnetically aligned.

On the basis of this, SANS and NMR studies of zwitterionic mixtures (both DMPC/DHPC and DMPC/CHAPSO), and the data obtained previously,^{22,29} one can conclude a general trend in the structural variation upon loss of the rim detergents as follows: bicelles \rightarrow ribbons (ribbon-meshed lamellae) \rightarrow perforated lamellae, consistent with TEM data reported previously.²⁸

In-Plane Structure of DMPC/DMPG/CHAPSO Lamellae.

Previous combined SANS and NMR studies on DMPC/DMPG/DHPC mixtures demonstrated that the fractional area of DHPC-rich perforations within the bilayer region could be estimated and that these perforations annealed with increased T .⁴⁴ A similar estimation can be made on the DMPC/DMPG/CHAPSO mixtures by comparing experimental versus calculated d spacings, given that at elevated temperatures lamellae are found at high concentration ($C_{lp} \geq 7.5$ wt %). Assuming homogeneously dispersed, nonperforated lamellae with small perturbations and thermal undulation, the theoretical d spacing, d_{cal} , of the lamellae can be roughly estimated to be d_b/ϕ_{lp} , where d_b and ϕ_{lp}

are the bilayer thickness (~ 40 Å for L_α DMPC) and the volume fraction of lipid, respectively, resulting in $d_{cal} \approx 160$ Å at 25 wt %. Using the d spacings detailed in Table 1, we can estimate the perforated to total area ratio from $f_p = (d_{cal} - d)/d_{cal}$, yielding a fractional perforated area of 35% at 330 K and $C_{lp} = 25$ wt %. Because similar d spacings are obtained for both $R = 0.01$ and 0.10, their in-plane percent perforations appear to be similar. The general trend of increasing experimental d spacing with increasing temperature suggests that a temperature-driven annealing of CHAPSO-rich perforations is occurring in a fashion similar to that observed with DHPC as CHAPSO migrates progressively from edge to planar regions.

With regard to the slightly charged DMPC/DMPG/CHAPSO mixture ($R = 0.01$), an estimation of the fraction of perforation as a function of progressive dilution, as described above, suggests little if any change in that fraction upon dilution (i.e., $f_p = 36\%$ at $C_{lp} = 25$ wt % decreasing to $f_p = 34\%$ at $C_{lp} = 7.5$ wt % at 330 K). Assuming that perforations are due to the CHAPSO resident in edge regions versus planar regions, there is no reason to expect this ratio to change with dilution. If anything, the overall CHAPSO associated with bicelles might decrease upon dilution, as per eq 5, which would predict a somewhat lower fractional area

of perforation upon dilution. For the highly charged ($R = 0.10$) DMPC/DMPG/CHAPSO mixtures, swelling upon dilution from $C_{lp} = 25$ to 7.5 wt % does not follow a straightforward 1-D dependence (i.e., $d \approx C_{lp}^{-0.66}$ at 330 K and $d \approx C_{lp}^{-0.76}$ at 340 K) as shown in Figures S3c and 4d, although higher-order Bragg peaks are clearly evident. Because there is no macroscopic phase separation, it is reasonable to assume that they remain homogeneously dispersed upon dilution. If applied uncritically, an analysis such as that described above would indicate that dilution increases the fractional area of perforations. As argued above, however, dilution is expected to decrease the fractional area of perforations. The temperature-induced structural segregation (one isotropic and the other alignable) observed in the ^{31}P NMR data (Figure 7) may provide some insight into this issue. Because DMPG promotes the retention of CHAPSO in DMPC (i.e., inhibiting the segregation), more defects are present in the membranes, presumably resulting in smaller d spacings. However, further study is needed to confirm this speculation.

Concentration Dependence and Charge Dependence of Disks and Ribbons. In the case of DMPC/DHPC mixtures, a disc-to-ribbon transition is found upon either dilution or increasing temperature,^{25,37} resulting from the loss of edge-localized DHPC. One significant difference in the DMPC/CHAPSO and DMPC/DHPC mixtures is that bicellar discs remain present even at quite low lipid concentrations (e.g., $C_{lp} = 0.25$ wt %), as confirmed by both SANS and TEM. This may again be attributed to the enhanced ability of CHAPSO, relative to DHPC, to mask the hydrocarbon chains of the long-chain amphiphiles from exposure to water. However, in the medium- C_{lp} sample (i.e., $C_{lp} = 2.5$ wt %), a ribbon phase is found at a low temperature sandwiched between discoidal bicelles at higher and lower concentrations (Figure 10a). Because the 0.25 wt % samples were prepared by diluting 25 wt % samples, it remains to be determined whether the discoidal morphology can be prepared by direct dilution from $C_{lp} = 2.5$ wt %, where the ribbon phase predominates to 0.25 wt %.

With respect to surface charge effects, it has been shown previously that DMPG effectively eliminates the ribbon phase, even at $R = 0.01$.^{21,47} In this study, a similar effect is observed in DMPC/DMPG/CHAPSO mixtures, with the exception that ribbons persist for the $C_{lp} = 2.5$ wt % case at $R = 0.01$. However, there is no evidence of ribbons once R is increased to 0.10.

Spontaneous Structural Diagrams. The current SANS data for high- C_{lp} samples demonstrate the thermal reversibility of the morphologies (Figure S3 in the Supporting Information). However, it has also been reported that lipid mixtures can be kinetically trapped in certain morphologies for long periods of time,⁶⁰ especially at low C_{lp} (<1 wt %). In the absence of certainty regarding the thermodynamically stable morphology, the structural diagrams presented in this section should be regarded as indicating spontaneous structures that arise when the samples are diluted to the indicated concentration from stock solutions at high C_{lp} (25 wt %) and low temperature (4 °C). It should also be noted that more than one structure may coexist even if a single structure is identified in the diagrams because its presence may overwhelm that of the others.

Figure 10a,c,d show the T - C_{lp} bicelle structural diagrams derived from SANS and NMR data for DMPC/DMPG/CHAPSO mixtures with $R = 0, 0.01$, and 0.10, respectively. In comparison to that of DMPC/DHPC as shown in Figure 10d,²⁵ the general range of morphological changes is similar. When sufficient edge-stabilizing detergent is available, smaller aggregates, such as discoidal bicelles, predominate. Loss of

detergents leads to larger aggregates such as ribbons, then to perforated lamellae, and eventually to MLVs or ULVs. The major differences between DHPC- and CHAPSO-containing mixtures lie in the location of boundaries of structural transitions, which occur at higher T and lower C_{lp} in CHAPSO-containing mixtures. This appears to be dictated by the preferential ability of CHAPSO versus DHPC to stabilize high-curvature edge regions. Whether this arises from CHAPSO's inherently higher partitioning from solution onto the bilayer edge (potentially important at low C_{lp}), its inherently greater ability to mask hydrophobic edges per molecule as a result of its different amphiphilic topography, or weaker miscibility with DMPC upon increasing temperature remains a question to be addressed.

The formation of ULVs and MLVs is hindered in the presence of higher surface charge density, possibly as a result of the consequent stiffening of the bilayer and interparticle Coulombic repulsion, respectively. Compared to DHPC, ribbons in the presence of CHAPSO are observed over a wider range of lipid concentrations and temperatures. Because the folding of planar structures into spherical ULVs/MLVs occurs when the edge line tension energy exceeds the bending energy of the bilayer, the preferred planar versus spherical morphologies in CHAPSO-containing mixtures is interpreted as a further manifestation of CHAPSO's enhanced stabilization of edge regions.

CONCLUSIONS

This study of CHAPSO-containing mixtures has focused on differences relative to DHPC-containing mixtures because both have been widely used for solubilizing and reconstituting membrane proteins, among other uses. Zwitterionic mixtures of either detergent undergo similar morphological transformations from discoidal bicelles to ribbons (or ribbon-meshed lamellae) and eventually to MLVs upon dilution or elevated T . The major difference is the higher stability of planar structures in the CHAPSO-containing mixtures, as evident from both SANS and ^{31}P NMR results. CHAPSO is clearly better than DHPC in stabilizing bicellar edge regions, but the precise origin of this difference will require further study. The addition of DMPG stabilizes smaller aggregates and tends to dampen differences between CHAPSO- and DHPC-containing mixtures. The spontaneous structural diagrams presented here provide a physical foundation for utilizing these mixtures in structural studies of membrane-associated proteins and elsewhere.

ASSOCIATED CONTENT

Supporting Information

Models used to fit the SANS data. Nanodisc morphology confirmed by transmission electron microscopy. Thermal reversibility of morphologies in high- C_{lp} DMPC/DMPG/CHAPSO mixtures. Temperature dependence of critical micelle concentrations of CHAPSO and DHPC. This material is available free of charge via the Internet at <http://pubs.acs.org>.

AUTHOR INFORMATION

Corresponding Authors

*E-mail: pm.macdonald@utoronto.ca.

*E-mail: mu-ping.nieh@ims.uconn.edu.

Notes

The authors declare no competing financial interest.

ACKNOWLEDGMENTS

M.-P.N. and M.L. acknowledge funding support from a UConn faculty large research grant and an NSF grant (CMMI 1131587) as well as technical support from the Canadian Neutron Beam Centre NRU (Chalk River, Ontario, Canada) and the Center for Structural Molecular Biology (CSMB) at ORNL for the use of their neutron spectrometers. P.M.M. gratefully acknowledges the support of the Natural Science and Engineering Research Council (NSERC) of Canada and the Canadian Challenge Fund for Innovation (CFI) for financial support of this research. J.K. acknowledges support from the Laboratory Directed Research and Development Program of Oak Ridge National Laboratory, managed by UT-Battelle, LLC, for the U.S. Department of Energy (DOE) under contract no. DE-AC05-00OR2275. This work also acknowledges additional support from the DOE Office of Biological and Environmental Research for the BioSANS instrument at the ORNL Center for Structural Molecular Biology and from the Scientific User Facilities Division of the DOE Office of Basic Energy Sciences for use of the High Flux Isotope Reactor (HFIR).

REFERENCES

- (1) Sanders, C. R.; Hare, B. J.; Howard, K. P.; Prestegard, J. H. Magnetically-Oriented Phospholipid Micelles as a Tool for the Study of Membrane-Associated Molecules. *Prog. Nucl. Magn. Reson. Spectrosc.* **1994**, *26*, 421–444.
- (2) Sanders, C. R.; Oxenoid, K. Customizing Model Membranes and Samples for NMR Spectroscopic Studies of Complex Membrane Proteins. *Biochim. Biophys. Acta, Biomembr.* **2000**, *1508*, 129–145.
- (3) Whiles, J. A.; Deems, R.; Vold, R. R.; Dennis, E. A. Bicycles in Structure—Function Studies of Membrane-Associated Proteins. *Bioorg. Chem.* **2002**, *30*, 431–442.
- (4) Sanders, C. R.; Kuhn Hoffmann, A.; Gray, D. N.; Keyes, M. H.; Ellis, C. D. French Swimwear for Membrane Proteins. *ChemBioChem* **2004**, *5*, 423–426.
- (5) De Angelis, A. A.; Jones, D. H.; Grant, C. V.; Park, S. H.; Mesleh, M. F.; Opella, S. J. NMR Experiments on Aligned Samples of Membrane Proteins. *Methods Enzymol.* **2005**, *394*, 350–382.
- (6) Katsaras, J.; Harroun, T. A.; Pencier, J.; Nieh, M.-P. Bicycellar Lipid Mixtures as used in Biochemical and Biophysical Studies. *Naturwissenschaften* **2005**, *92*, 355–366.
- (7) Marcotte, L.; Auger, M. Bicycles as Model Membranes for Solid- and Solution-State NMR Studies of Membrane Peptides and Proteins. *Concepts Magn. Reson.* **2005**, *24A*, 17–37.
- (8) Sanders, C. R.; Sönnichsen, F. Solution NMR of Membrane Proteins: Practice and Challenges. *Magn. Reson. Chem.* **2006**, *44*, S24–S40.
- (9) Poget, S. F.; Girvin, M. E. Solution NMR of Membrane Proteins in Bilayer Mimics: Small is Beautiful, but Sometimes Bigger is Better. *Biochim. Biophys. Acta, Biomembr.* **2007**, *1768*, 3098–3106.
- (10) Kim, H. J.; Howell, S. C.; Van Horn, W. D.; Jeon, Y. H.; Sanders, C. R. Recent Advances in the Application of Solution NMR Spectroscopy to Multi-Span Integral Membrane Proteins. *Prog. Nucl. Magn. Reson. Spectrosc.* **2009**, *55*, 335–360.
- (11) Dürr, U. H. N.; Goldenberg, M.; Ramamoorthy, A. The Magic of Bicycles Lights Up Membrane Protein Structure. *Chem. Rev.* **2012**, *112*, 6054–6074.
- (12) Dave, P. C.; Inbaraj, J. J.; Lorigan, G. A. Electron Paramagnetic Resonance Studies of Magnetically Aligned Phospholipid Bilayers Utilizing a Phospholipid Spin Label. *Langmuir* **2004**, *20*, 5801–5808.
- (13) Nusair, N. A.; Lorigan, G. A. Investigating the Structural and Dynamic Properties of n-Doxylstearic Acid in Magnetically-Aligned Phospholipid Bilayers by X-Band EPR Spectroscopy. *Chem. Phys. Lipids* **2005**, *133*, 151–164.
- (14) Cardon, T. B.; Dave, P. C.; Lorigan, G. A. Magnetically Aligned Phospholipid Bilayers with Large q Ratios Stabilize Magnetic Alignment with High Order in the Gel and $L\alpha$ Phases. *Langmuir* **2005**, *21*, 4291–4298.
- (15) Faham, S.; Bowie, J. U. Bicycell Crystallization: A New Method for Crystallizing Membrane Proteins Yields a Monomeric Bacteriorhodopsin Structure. *J. Mol. Biol.* **2002**, *316*, 1–6.
- (16) Ujwal, R.; Bowie, J. U. Crystallizing Membrane Proteins Using Lipidic Bicycles. *Methods* **2011**, *55*, 337–341.
- (17) Johansson, L. C.; Wöhri, A. B.; Katona, G.; Engström, S.; Neutze, R. Membrane Protein Crystallization from Lipidic Phases. *Curr. Opin. Struct. Biol.* **2009**, *19*, 372–378.
- (18) Kang, C.; Vanoye, C. G.; Welch, R. C.; Van Horn, W. D.; Sanders, C. R. Functional Delivery of a Membrane Protein into Oocyte Membranes Using Bicycles. *Biochemistry* **2010**, *49*, 653–655.
- (19) Barbosa-Barros, L.; Rodríguez, G.; Barba, C.; Cócera, M.; Rubio, L.; Estelrich, J.; López-Iglesias, C.; de la Maza, A.; López, O. Bicycles: Lipid Nanostructured Platforms with Potential Dermal Applications. *Small* **2012**, *8*, 807–818.
- (20) Morigaki, K.; Kimura, S.; Okada, K.; Kawasaki, T.; Kawasaki, K. Formation of Substrate-Supported Membranes from Mixtures of Long- and Short-Chain Phospholipids. *Langmuir* **2012**, *28*, 9649–9655.
- (21) Nieh, M.-P.; Glinka, C. J.; Krueger, S.; Prosser, R. S.; Katsaras, J. SANS Study on the Effect of Lanthanide Ions and Charged Lipids on the Morphology of Phospholipid Mixtures. *Biophys. J.* **2002**, *82*, 2487–2498.
- (22) Nieh, M.-P.; Glinka, C. J.; Harroun, T. A.; Pabst, G.; Katsaras, J. Magnetically Alignable Phase of Phospholipid “Bicycle” Mixtures Is a Chiral Nematic Made Up of Wormlike Micelles. *Langmuir* **2004**, *20*, 7893–7897.
- (23) Sanders, C. R.; Schwonek, J. P. Characterization of Magnetically Orientable Bilayers in Mixtures of Dihexanoylphosphatidylcholine and Dimyristoylphosphatidylcholine by Solid-State NMR. *Biochemistry* **1992**, *31*, 8898–8905.
- (24) Ottiger, M.; Bax, A. Characterization of Magnetically Oriented Phospholipid Micelles for Measurement of Dipolar Couplings in Macromolecules. *J. Biomol. NMR* **1998**, *12*, 361–372.
- (25) Picard, F.; Paquet, M.-J.; Levesque, J.; Bélanger, A.; Auger, M. ³¹P NMR First Spectral Moment Study of the Partial Magnetic Orientation of Phospholipid Membranes. *Biophys. J.* **1999**, *77*, 888–902.
- (26) Triba, M. N.; Warschawski, D. E.; Devaux, P. F. Reinvestigation by Phosphorus NMR of Lipid Distribution in Bicycles. *Biophys. J.* **2005**, *88*, 1887–1901.
- (27) Soong, R.; Macdonald, P. M. Water Diffusion in Bicycles and the Mixed Bicycle Model. *Langmuir* **2009**, *25*, 380–390.
- (28) Van Dam, L.; Karlsson, G.; Edwards, K. Direct Observation and Characterization of DMPC/DHPC Aggregates Under Conditions Relevant for Biological Solution NMR. *Biochim. Biophys. Acta, Biomembr.* **2004**, *1664*, 241–256.
- (29) Sanders, C. R.; Prestegard, J. H. Magnetically Orientable Phospholipid Bilayers Containing Small Amounts of a Bile Salt Analogue, CHAPSO. *Biophys. J.* **1990**, *58*, 447–460.
- (30) Sanders, C. R.; Prestegard, J. H. Orientation and Dynamics of .beta.-Dodecyl Glucopyranoside in Phospholipid Bilayers by Oriented Sample NMR and Order Matrix Analysis. *J. Am. Chem. Soc.* **1991**, *113*, 1987–1996.
- (31) Sanders, C. R.; Landis, G. C. Reconstitution of Membrane Proteins into Lipid-Rich Bilayered Mixed Micelles for NMR Studies. *Biochemistry* **1995**, *34*, 4030–4040.
- (32) Czernski, L.; Sanders, C. R. Functionality of a Membrane Protein in Bicycles. *Anal. Biochem.* **2000**, *284*, 327–333.
- (33) Cavagnero, S.; Dyson, H. J.; Wright, P. E. Improved Low pH Bicycle System for Orienting Macromolecules over a Wide Temperature Range. *J. Biomol. NMR* **1999**, *13*, 387–391.
- (34) Wang, H.; Eberstadt, M.; Olejniczak, E. T.; Meadows, R. P.; Fesik, S. W. A Liquid Crystalline Medium for Measuring Residual Dipolar Couplings over a Wide Range of Temperatures. *J. Biomol. NMR* **1998**, *12*, 443–446.
- (35) Nieh, M.-P.; Yamani, Z.; Kučerka, N.; Katsaras, J.; Burgess, D.; Breton, H. Adapting a Triple-Axis Spectrometer for Small Angle

Neutron Scattering Measurements. *Rev. Sci. Instrum.* **2008**, *79*, 095102-1–095102-6.

(36) Kline, S. R. Reduction and Analysis of SANS and USANS Data Using IGOR Pro. *J. Appl. Crystallogr.* **2006**, *39*, 895–900.

(37) Soong, R.; Nieh, M.-P.; Nicholson, E.; Katsaras, J.; Macdonald, P. M. Bicellar Mixtures Containing Pluronic F68: Morphology and Lateral Diffusion from Combined SANS and PFG NMR Studies. *Langmuir* **2010**, *26*, 2630–2638.

(38) Tanner, J. E. Use of the Stimulated Echo in NMR Diffusion Studies. *J. Chem. Phys.* **1970**, *52*, 2523.

(39) Fauth, J.-M.; Schweiger, A.; Braunschweiler, L.; Forrer, J.; Ernst, R. R. Elimination of Unwanted Echoes and Reduction of Dead Time in Three-Pulse Electron Spin-Echo Spectroscopy. *J. Magn. Reson.* **1986**, *66*, 74–85.

(40) Mills, R. Self-Diffusion in Normal and Heavy Water in the Range 1–45°. *J. Phys. Chem.* **1973**, *77*, 685–688.

(41) Tristram-Nagle, S.; Liu, Y.; Legleiter, J.; Nagle, J. F. Structure of Gel Phase DMPC Determined by X-ray Diffraction. *Biophys. J.* **2002**, *83*, 3324–3335.

(42) Losonczi, J. A.; Prestegard, J. H. Improved Dilute Bicelle Solutions for High-Resolution NMR of Biological Macromolecules. *J. Biomol. NMR* **1998**, *12*, 447–451.

(43) Nieh, M.-P.; Raghunathan, V. A.; Kline, S. R.; Harroun, T. A.; Huang, C.-Y.; Pencer, J.; Katsaras, J. Spontaneously Formed Unilamellar Vesicles with Path-Dependent Size Distribution. *Langmuir* **2005**, *21*, 6656–6661.

(44) Hayter, J. B.; Penfold, J. J. Determination of Micelle Structure and Charge by Neutron Small-Angle Scattering. *Colloid Polym. Sci.* **1983**, *261*, 1022–1030.

(45) Seelig, J. ³¹P Nuclear Magnetic Resonance and the Head Group Structure of Phospholipids in Membranes. *Biochim. Biophys. Acta* **1978**, *515*, 105–140.

(46) Scholz, F.; Boroske, E.; Helfrich, W. Magnetic Anisotropy of Lecithin Membranes. A New Anisotropy Susceptometer. *Biophys. J.* **1984**, *45*, 589–592.

(47) Nieh, M.-P.; Raghunathan, V. A.; Pabst, G.; Harroun, T.; Nagashima, K.; Morales, H.; Katsaras, J.; Macdonald, P. M. Temperature Driven Annealing of Perforations in Bicellar Model Membranes. *Langmuir* **2011**, *27*, 4838–4847.

(48) Von Berlepsch, H. Weakly Charged Lamellar Bilayer System: Interplay Between Thermal Undulations and Electrostatic repulsion. *Eur. Phys. J. E* **2000**, *1*, 141–152.

(49) Winterhalter, M.; Helfrich, W. Effect of Surface Charge on the Curvature Elasticity of Membranes. *J. Phys. Chem.* **1988**, *92*, 6865–6867.

(50) Mitchell, D. J.; Ninham, B. W. Curvature Elasticity of Charged Membranes. *Langmuir* **1989**, *5*, 1121–1123.

(51) Macdonald, P. M.; Soong, R. Diffusion NMR and Bicelle Morphology. *Can. J. Chem.* **2011**, *89*, 1021–1035.

(52) Callaghan, P. T.; Söderman, O. Examination of the Lamellar Phase of Aerosol OT-Water Using Pulsed Field Gradient Nuclear Magnetic Resonance. *J. Phys. Chem.* **1983**, *87*, 1737–1744.

(53) Lindblom, G.; Orädd, G. NMR Studies of Translational Diffusion in Lyotropic Liquid Crystals and Lipid Membranes. *Prog. Nucl. Magn. Reson. Spectrosc.* **1994**, *26*, 483–515.

(54) Soong, R.; Macdonald, P. M. Diffusion of PEG Confined between Lamellae of Negatively Magnetically Aligned Bicelles: Pulsed Field Gradient ¹H NMR Measurements. *Langmuir* **2008**, *24*, 518–527.

(55) Polozova, A.; Dubachev, G.; Simonova, T.; Barsukov, L. Temperature-Induced Micellar-Lamellar Transformation in Binary Mixtures of Saturate Phosphatidylcholines with Sodium Cholate. *FEBS Lett.* **1995**, *358*, 17–22.

(56) Heerklotz, H.; Seelig, J. Correlation of Membrane/Water Partition Coefficient of Detergents with the Critical Micelle Concentration. *Biophys. J.* **2000**, *78*, 2435–2440.

(57) Tausk, R. J. M.; Karmiggelt, J.; Oudshoorn, C.; Overbeek, J. Physical Chemical Studies of Short Chain Lecithin Homologues. I. Influence of the Chain Length of the Fatty Acid Ester and of Electrolytes on the Critical Micelle Concentration. *Biophys. Chem.* **1974**, *1*, 175–183.

(58) Lichtenberg, D.; Opatowski, E.; Kozlov, M. Phase Boundaries in Mixtures of Membrane-Forming Amphiphiles and Micelle-Forming Amphiphiles. *Biochim. Biophys. Acta* **2000**, *1508*, 1–19.

(59) Lichtenberg, D.; Ahlyayauch, H.; Alonso, A.; Goñi, F. Detergent Solubilization of Lipid Bilayers: a Balance of Driving Forces. *TIBS* **2012**, *38*, 85–93.

(60) Nieh, M.-P.; Harroun, T. A.; Raghunathan, V. A.; Glinka, C. J.; Katsaras, J. Concentration-Independent Spontaneously Forming Biomimetic Vesicles. *Phys. Rev. Lett.* **2003**, *91*, 158105.